Absorptivity Modulation with Salisbury-Inspired Structures for X-Band

Xhoandri Lleshi, Thi Quynh van Hoang, Paolo Martins, Brigitte Loiseaux, Didier Lippens

Absorptivity Modulation with Salisbury-Inspired Structures for X-Band

Xhoandri Lleshi*†, Thi Quynh Van Hoang*, Paolo Martins*, Brigitte Loiseaux*, Didier Lippens†
*Thales Research and Technology, Palaiseau, France, van.hoang@thalesgroup.com
†Institut d'Electronique, de Microélectronique et de Nanotechnologie, Lille, France

***Abstract*—Absorptivity control is a very desired feature in many RF applications as it allows enhancing electromagnetic performances such as antenna radiation patterns and reducing radar cross section. In this paper, two Salisbury-inspired structures with absorption level of 20% and 50% in X-band frequencies (8 – 12 GHz) are presented. Both structures are fabricated by electron beam evaporation technique with Nickel Chrome as material for the resistive coating on PEKK dielectric substrates, which are manufactured by thermal compressing. The RF characterization in non-anechoic environment confirms the results obtained by numerical computations. For both vertical and horizontal polarizations, quasi-perfect agreement over the frequency band of interest is found with a maximal variation of the absorptivity less than 5% between the center frequency at 10 GHz and the edges frequencies at 8 GHz and 12 GHz. The absorption behavior of the two structures was also evaluated under oblique incidence.**

***Index Terms*—Absorptivity control, E-beam deposition, RF absorbers, resistive screen.**

I. Introduction

Controlling diffraction and scattering of antenna systems is one of the most desired functions in the RF domain since this allows reducing the radar cross section (RCS), obtaining a low-observability, attenuating antenna back-scatterings, mitigating interferences between nearby systems, etc. Different methods have been proposed in the literature to reduce the RCS. Many studies exploit checkerboard configurations in which the basic principle is the modulation of the reflection phase of a structure to modify the directions of the scattered fields. Toward this goal, metamaterials alternating two Electromagnetic Band Gap (EBG) materials with square and circular patterns are presented in [1]. Other solutions are implemented with Artificial Magnetic Conductors (AMC) [2] and magnetic materials [3]. For the back-scattering reduction and the interference mitigation, a novel approach is to use semitransparent architectures made of resistive layers with operation principle similar to the well-known resistive cards (R-cards) [4]–[7]. This approach relies on the gradual impedance matching of resistive elements to a metal plate or the free space.

In this paper, resistive screens for absorptivity modulation are presented. The structures are inspired from the Salisbury screen with the modulation of the surface resistance to obtain absorption levels from 0.1 (10%-absorptivity) to 1.0 (100%-absorptivity) targeting X-band operation with a maximum ripple of less than 5%. The paper is organized as follows: in section II, the details of the design are explained and the surface resistances required for targeted absorption levels are computed. Section III presents two fabricated prototypes for absorption levels of 0.2 and 0.5 and the characterization of their surface resistances. In section IV, the comparison between simulation and characterization, in a non-anechoic environment, for normal and oblique incidences is presented.

II. Absorptivity Modulation with Salisbury-Inspired Absorbers

The resistive screen absorbers proposed in this paper are inspired from the well-known Salisbury absorber, which was patented in 1952 [8]. It is a resonant structure composed of three layers: a metallic layer acting as a ground plane, thus avoiding transmission, a dielectric spacer with a thickness d, and a purely resistive sheet with a surface resistance R_s that matches free space impedance, as depicted in Fig. 1. When an electromagnetic wave impinges onto the 377 Ω resistive sheet under normal incidence, it passes through it, forming a standing wave with the 180° phase-shifted wave reflected from the ground plane. This configuration occurs when the double path phase-shift in the dielectric spacer and the phase-shift π introduced by the metal plate at the bottom satisfies (1):

$$\Delta\phi = 2(\frac{2\pi}{\lambda_g}d) + \pi = 2\pi \tag{1}$$

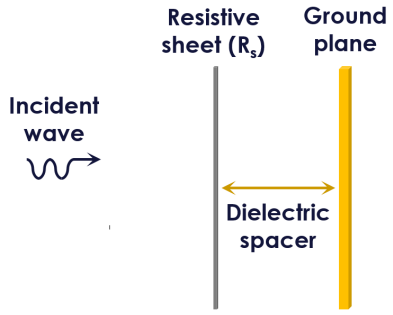

Fig. 1. Schematic design of a resistive screen absorber.

The double path phase-shift must equal π, thus d must be $\lambda_g/4$ (where λ_g refers to the wavelength of the absorbed resonant frequency in the dielectric). This condition ensures that the two waves are in phase at $\lambda_g/4$ apart from the metal

plate with the E-field being twice the intensity of the initial field [9]. Since the resistive sheet is placed at this point, the energy of the wave is entirely dissipated by the resistive losses [10].

Based on this principle, by adjusting the surface resistance of the resistive screen, one can modulate the absorption level between a few percent and 100% at the center frequency. To determine the surface resistance, the schematic of a resistive screen absorber in Fig. 2 is used. The input impedance Z_{in} for a lossless dielectric layer of thickness d is calculated as follow:

$$Z_{in}(f) = jZ_d tan(2\pi\sqrt{\varepsilon\mu_0} f d) \tag{2}$$

where $Z_d = \sqrt{\mu_0/\varepsilon}$ (in Ω) is the characteristic impedance of the dielectric, $\varepsilon = \varepsilon_r\varepsilon_0$ is the dielectric spacer permittivity (in F/m), μ_0 is the free space permeability (in H/m), and f is the frequency.

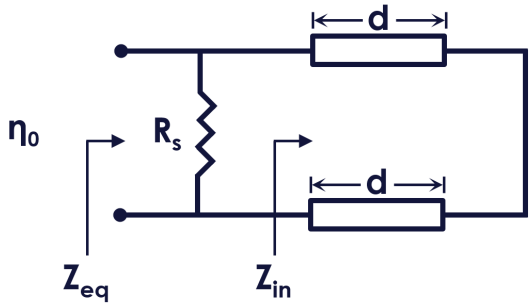

Fig. 2. Equivalent transmission line model of a resistive screen absorber.

The reflection coefficient as a function of the frequency can be expressed as in (3):

$$\Gamma(f) = \frac{Z_{eq}(f) - \eta_0}{Z_{eq}(f) + \eta_0} \tag{3}$$

where η_0 is the characteristic impedance of the free space equal to $377\,\Omega$, and Z_{eq} is the equivalent impedance of the surface resistance R_s in parallel with the input impedance Z_{in}. With a thickness $d = \lambda_g/4$ and at the resonant frequency f_0, the equivalent impedance equals to the surface resistance R_s so that (3) is reduced to:

$$\Gamma(f_0) = \frac{R_s - \eta_0}{R_s + \eta_0} \tag{4}$$

By changing the reflection coefficient one can target a specific absorption level A following the energy conservation law $A(f) = 1 - |\Gamma(f)|^2$, by noting that no transmission occurs due to the ground plane. The required surface resistance for a targeted absorption level is found by:

$$R_s = \eta_0 \frac{1 + \sqrt{1 - A(f_0)}}{1 - \sqrt{1 - A(f_0)}} \tag{5}$$

This simple formula allows finding the resistance value for any absorption level without massive full-wave simulations. In Table I, the computed surface resistance values using (5) are presented, for target absorption levels from 0.1 to 1.0 along with the corresponding reflection coefficient.

TABLE I
TARGET ABSORPTIVITY VALUES RANGING FROM 0.1 TO 1.0 AND THE CORRESPONDING REFLECTION COEFFICIENTS AND REQUIRED SURFACE RESISTANCES.

Target absorptivity A	**Reflection coefficient** Γ	**Surface resistance** $R_s(\Omega/sq)$
0.1	0.95	10
0.2	0.90	21
0.3	0.83	34
0.4	0.77	48
0.5	0.71	64
0.6	0.63	85
0.7	0.55	110
0.8	0.44	145
0.9	0.31	200
1.0	0.03	358

We note that, the surface resistance value for the targeted unitary absorption is $358\,\Omega/sq$, which is less than the one in the Salisbury perfect matching value of $377\,\Omega/sq$, with an absorptivity of 0.99 instead of 1.0. The reason is related to the variation of the absorptivity with respect to the frequency. A perfect Salisbury screen introduces more absorptivity variations than a slightly mismatched resistive screen for frequencies f different from the resonant one f_0.

The simulations under normal incidence for targeted absorption levels in Table I are plotted in Fig. 3.

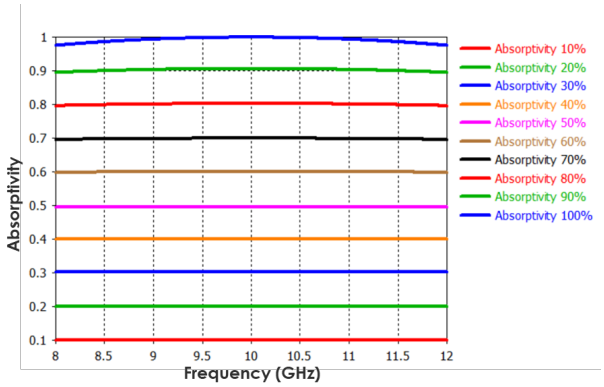

Fig. 3. Simulated frequency dependence of different absorptivity from 0.1 (10%) to 1.0 (100%).

The absorptivity up to 0.8 is perfectly flat in the whole frequency band, then, a slight variation is visible between levels from 0.8 to 1.0. The most significant variation of 2.5% is observed at 8 GHz and 12 GHz, where absorptivity is 97.5% rather than 100%. Equation (4) is analyzed to understand this variation in frequency of the absorption level. When the dielectric slab has a physical thickness of a quarter-wavelength, Z_{in} becomes infinite and $Z_{eq} = R_s$. This condition is satisfied only at the center frequency f_0 of 10 GHz. At the frequency edges, the quarter-wavelength condition is no longer satisfied and the equivalent impedance Z_{eq} is computed as the parallel between Z_{in} and R_s that reduces the absorptivity.

An advantage using such resistive screens is that one could use the same values of surface resistances for any frequency band to absorb the same amount of energy. Only the dielectric spacer thickness d and permittivity ε_r need to be changed to satisfy the quarter-wavelength condition.

III. Fabricated Prototypes

Two prototypes are fabricated to experimentally validate the concept of modulating the absorption level using Salisbury-inspired resistive screen structures: one with $21\,\Omega/sq$ to obtain 20% absorptivity, depicted in Fig. 4(a), and the other with $64\,\Omega/sq$ to obtain 50% absorptivity, shown in Fig. 4(b). The two $25\,cm\times\ 25\,cm$ structures consist of a copper plate at the bottom, a 4.2mm-thick PEKK dielectric spacer (with $\varepsilon_r^{'} = 3.3$), which corresponds to $\lambda_g/4$ at the center frequency at 10 GHz, and a Nickel Chrome (NiCr) coating resistive screen on the top.

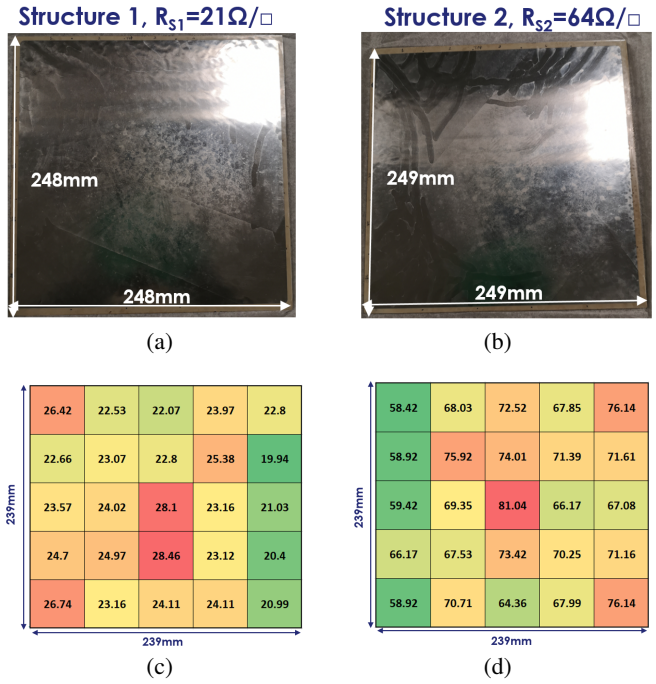

Fig. 4. Prototypes fabricated with the electron beam evaporation technique. Top views of (a) Structure 1 with $21\,\Omega/sq$, and (b) Structure 2 with $64\,\Omega/sq$. The cartography of the surface resistance values in (c) and (d), respectively for Structure 1 and Structure 2. Green and red colors correspond to the minimum and maximum characterized resistive values, respectively.

PEKK thermoplastic substrates are manufactured by thermal compressing with temperatures around 320 – 380°C by the platform Canoe [11]. Resistive screens and copper ground plane are deposited by electron beam (E-beam) evaporation technique, in clean room by Neyco company [12]. One of the novelties introduced in this article is the exploitation of the E-beam on a thermoplastic, which is not commonly used for this technique. For the ground plate, a thin copper layer of $2\,\mu m$ is deposited. Nickel Chrome is used for the resistive screens by controlling the thickness, which defines the sheet resistance value as following:

$$R_s = \frac{\rho}{t} \tag{6}$$

where ρ is the NiCr resistivity (in $\Omega.m$) and t is the resistive screen thickness (in m). The thicknesses are 67 nm and 25 nm, with an error of $\pm 5\%$, for the surface resistances of $21\,\Omega/sq$ and $64\,\Omega/sq$, respectively.

The cartographies of the surface resistances are given for Structure 1 in Fig. 4(c) and for Structure 2 in Fig. 4(d). The values are retrieved from the characterization using a 4-point probes method [13]. Both prototypes have been virtually divided into 25 zones. For each zone, the resistance value is retrieved from the average value of three different measurements in regions close to the zone center. For Structure 1, the average measured sheet resistance value of $23.69\,\Omega/sq$ is comparable to the stated value of $21\,\Omega/sq$ from the manufacturer (variation of 13%). For Structure 2, the average value of $68.98\,\Omega/sq$ found by measurement is quite similar to the expected value of $64\,\Omega/sq$ stated by the supplier (variation of 8%).

It is worth noting that for both structures, the average resistance value varies along the horizontal direction, from $24.8\,\Omega/sq$ in the first column to $21.03\,\Omega/sq$ in the last column for Structure 1, and from $60.37\,\Omega/sq$ in the first column to $72.42\,\Omega/sq$ in the last column for Structure 2. However, along the vertical direction, the average resistance values of different rows remain similar. The difference of resistance distribution between horizontal and vertical directions could lead to different absorption characteristics in horizontal and vertical polarizations.

IV. Simulation and Characterization

As seen before, the energy conservation allows the computation of the absorptivity $A(f) = 1–|\Gamma(f)|^2$. For the simulation, a MATLAB code is used to calculate the reflection coefficient given by (3) for normal incidence. For oblique incidences, the incident angle θ is considered and (3) is written as (7a) for vertical polarization (V-pol.), and as (7b) for horizontal polarization (H-pol.):

$$\Gamma_{Vpol.}(f) = \frac{Z_{eq} - \eta_0/cos\theta}{Z_{eq} + \eta_0/cos\theta} \tag{7a}$$

$$\Gamma_{Hpol.}(f) = \frac{Z_{eq} - \eta_0 cos\theta}{Z_{eq} + \eta_0 cos\theta} \tag{7b}$$

The setup used for the reflection coefficient measurement under normal and oblique incidences is depicted in Fig. 5. It is composed of one arm fixed to a rigid sample holder that supports the absorbing screen and a second arm that can rotate. Two Satimo QR2000 horn antenna [14] are used as the transmitter (Tx) and receiver (Rx) and are placed 57.5 cm apart from the central support. Two dielectric lenses (one for each arm) are used and provide an additional directivity gain of 5 – 15 dB for both vertical and horizontal polarizations in the frequency range of 6 – 16 GHz.

The calculation of the reflection coefficient of the absorber under test (AUT) is performed with (8) [15], and a time-gating is applied to the measured signals in post-processing.

$$\Gamma^{AUT}(f) = \frac{S_{i1}^{total} - S_{i1}^{freespace}}{S_{i1}^{freespace} - S_{i1}^{metal}} \tag{8}$$

where S_{i1} is the scattering parameter, $total$ refers to the measurement when the absorber is placed on the support, $freespace$ refers to free space when no structure is located on the support, and $metal$ refers to a metal plate with the same dimensions as the ones of the absorber under test. When normal incidence is measured, $i = 1$, only antenna 1 is used as Tx and Rx. When oblique incidences are considered, $i = 2$ and antenna 1 is the Tx while antenna 2 is the Rx.

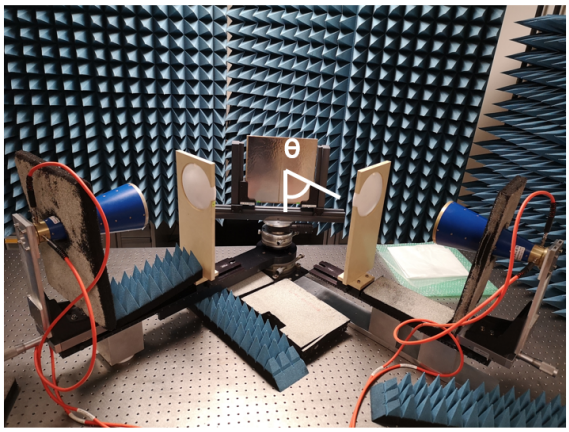

Fig. 5. RF characterization setup composed of two horn antennas (Satimo QR2000) and two lenses. Various foam absorbers are located close to critical reflection surfaces to avoid spurious reflected signals.

A. Normal incidence

The comparison between the simulation and the characterization result for vertical polarization and horizontal polarization is depicted in Fig. 6(a) for Structure 1 and in Fig. 6(b) for Structure 2.

A quasi-flat response is found for the experimental results for Structure 1, for both polarizations. In addition, the results are comparable to those obtained by simulation with $R_{s,average}$ confirming the homogeneity of the structure around the value of $23.7\,\Omega/sq$. Considering Structure 2, one can note that the characterization for vertical polarization has an absorptivity of around 55%, while horizontal absorptivity has a value of 60%. This difference is related to the different resistance values pointed out in Section III. For V-pol., the bottom and top sides of the structure have similar average values of $67.62\,\Omega/sq$ and $68.59\,\Omega/sq$, while for H-pol., the average values from left to the right side are $60.37\,\Omega/sq$ and $72.42\,\Omega/sq$.

B. Oblique incidence

For Structure 1, Fig. 7 shows that simulations, on the left, and characterizations, on the right, exhibit similar behavior for both V-pol. and H-pol.. One can note a singularity for V-pol. around 7 GHz that is difficult to explain due to possible measurement inaccuracy or fabrication imperfections. For V-pol., angular robustness is maintained up to 30° for a target absorptivity of 20%, as demonstrated by the flat X-band behavior, whereas for H-pol., a different behavior is observed, with the absorption level increasing with incident angle as expected from (7b).

For Structure 2, the characterization (right) and simulation (left) plots are depicted in Fig. 8. For H-pol., similar behavior is obtained with high absorptivity for high incident angles following (7b). For V-pol., we notice in Fig. 8(b) a shift of the center frequency toward high frequency around 13 GHz and an unexpected behavior at low frequency between 6 and 8 GHz. For the first issue, the explanation could be attributed to the fact that the PEKK dielectric layer has a permittivity value lower than the stated value of 3.3. This real value has not retrieved from a characterization stage yet. For the second issue, it might be related to measurement inaccuracy as for Structure 1. Nevertheless, the response over the X-band is flat up to incident angles of 28° for an absorptivity of 50%.

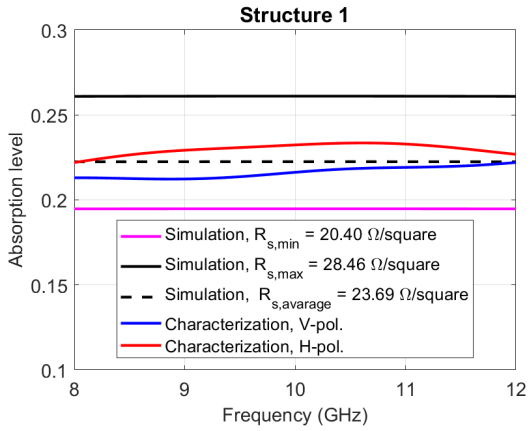

(a)

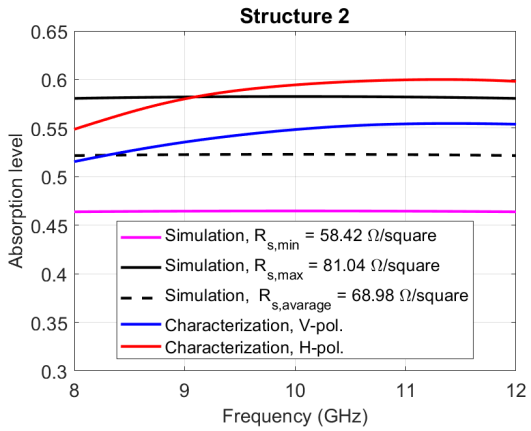

(b)

Fig. 6. Simulation for the minimum surface resistance value (solid line in violet), maximum resistance value (solid line in black), average value (dashed line in black), and the characterization results for vertical polarization (curve in blue) and horizontal polarization (curve in red).

In conclusion, both single resistive screen structures satisfy flat absorptivity levels of 20% up to $\theta = 30°$ for Structure 1 and of 50% up to $\theta = 28°$ for Structure 2, for vertical polarization.

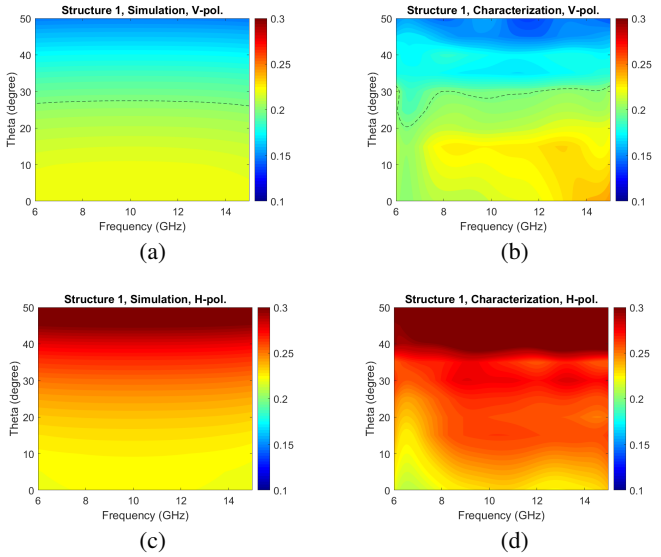

Fig. 7. Cartography of the absorptivity in the frequency range of 6 – 15 GHz and for incident angles from 0° to 50° for Structure 1. (a) and (b) correspond to the simulation and characterization for V-pol., respectively. (c) and (d) correspond to the simulation and characterization for H-pol., respectively.

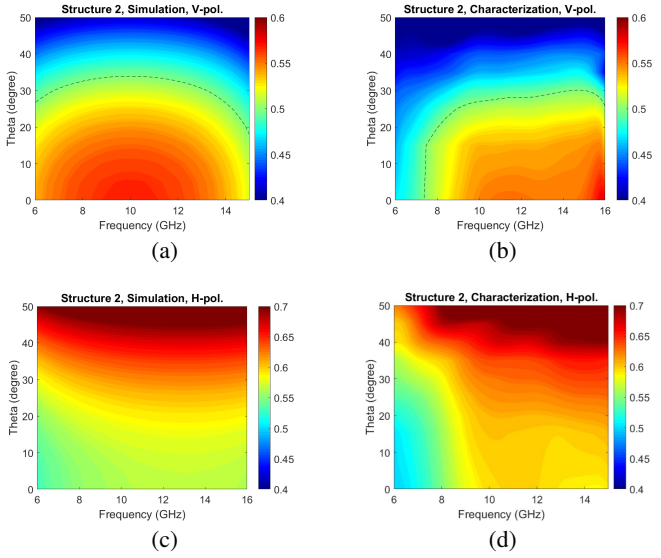

Fig. 8. Cartography of the absorptivity in the frequency range of 6 – 15 GHz and for incident angles from 0° to 50° for Structure 2. (a) and (b) correspond to the simulation and characterization for V-pol., respectively. (c) and (d) correspond to the simulation and characterization for H-pol., respectively.

V. Conclusion

In this paper, two fabricated Salisbury-inspired prototypes able to absorb 20% and 50% of the energy of an electromagnetic incident wave in X-band were presented. The design of the three-layer structure composed of a ground plane, a $\lambda_g/4$-thick dielectric spacer and a resistive film was analyzed and the required surface resistances for targeted absorption levels were computed. These values were found to be frequency independent with the same absorption levels that can be obtained for different operating bands by simply changing the dielectric thickness or permittivity. In a second step, the fabrication of two prototypes by using electron beam evaporation technique to deposit the resistive layer with Nickel Chrome was presented. The characterization of such structures confirmed the flat response obtained by numerical computation. In the future, the contribution of industrial techniques as Roll to Roll (R2R) will allow mass production of such resistive screens targeting different absorption levels. To increase the bandwidth, multilayered structures can be designed and optimization algorithms could allow retrieving the best combination of the number of layers, dielectric properties and thicknesses of the different spacers.

Acknowledgment

This work has been partly funded by the French MOD. The authors would like to thank Carole Jégou, Philippe Pouliguen and Sylvain Gransart for their helpful technical discussions.

References

[1] W. Chen, C. A. Balanis, and C. R. Birtcher, "Checkerboard ebg surfaces for wideband radar cross section reduction," *IEEE Transactions on Antennas and Propagation*, vol. 63, no. 6, pp. 2636–2645, 2015.

[2] A. Y. Modi, C. A. Balanis, C. R. Birtcher, and H. N. Shaman, "Novel design of ultrabroadband radar cross section reduction surfaces using artificial magnetic conductors," *IEEE Transactions on Antennas and Propagation*, vol. 65, no. 10, pp. 5406–5417, 2017.

[3] W. Li, Y. Zhang, T. Wu, J. Cao, Z. Chen, and J. Guan, "Broadband radar cross section reduction by in-plane integration of scattering metasurfaces and magnetic absorbing materials," *Results in Physics*, vol. 12, pp. 1964–1970, 2019. [Online]. Available: https://www.sciencedirect.com/science/article/pii/S2211379719303298

[4] K. Klionovski, "Scattering of toroidal waves by semitransparent reflectors of revolution in application to omnidirectional antennas," *IEEE Transactions on Antennas and Propagation*, vol. 69, no. 3, pp. 1610–1620, 2021.

[5] M. Mahmoud, T.-H. Lee, and W. Burnside, "Enhanced compact range reflector concept using an r-card fence: two-dimensional case," *IEEE Transactions on Antennas and Propagation*, vol. 49, no. 3, pp. 419–428, 2001.

[6] L. Du and Y. Fu, "A small wideband low-multipath gnss antenna using resistive film," *IEEE Antennas and Wireless Propagation Letters*, vol. 12, pp. 1045–1048, 2013.

[7] D. Archer, "Artificial resistive card," US Patent 5 126 716, Mesa, AZ, Jun. 30, 1992.

[8] W. Salisbury, "Absorbent body for electromagnetic waves," U.S. patent 2 599 944, Jun. 10, 1952.

[9] D. M. Pozar, *Microwave Engineering, 4th ed.* USA: Wiley, 2011.

[10] R. Fante and M. McCormack, "Reflection properties of the salisbury screen," *IEEE Transactions on Antennas and Propagation*, vol. 36, no. 10, pp. 1443–1454, 1988.

[11] Canoe, "www.platefrome-canoe.com."

[12] Neyco, "www.neyco.fr."

[13] F. M. Smits, "Measurement of sheet resistivities with the four-point probe," *The Bell System Technical Journal*, vol. 37, no. 3, pp. 711–718, 1958.

[14] "https://www.mvg-world.com/fr/products/antennas/measurement-probes-and-feeds/closed-boundary-quad-ridge-horns."

[15] X. Lleshi, T. Q. Van Hoang, B. Loiseaux, and D. Lippens, "Design and full characterization of a 3-d-printed hyperbolic pyramidal wideband microwave absorber," *IEEE Antennas and Wireless Propagation Letters*, vol. 20, no. 1, pp. 28–32, 2021.